ACS OMEGA

Open Access

http://pubs.acs.org/journal/acsodf

Article

Modeling and Experimental Investigation of Sulfurous Compounds Removal from Gas Condensate through Ultrasound-Assisted Oxidative Desulfurization Method

Ameneh Taghizadeh, Maryam Asemani,* Feridun Esmaeilzadeh, and Abolhasan Ameri

Cite This: *ACS Omega* 2023, 8, 42522−42539

Read Online

ACCESS | Metrics & More | Article Recommendations

ABSTRACT: This study employed an ultrasound-assisted oxidative desulfurization process (UAOD) to investigate the degradation of three sulfurous compounds in the synthetic gas condensate. Various parameters, including oxidizers (hydrogen peroxide, sodium peroxide, potassium superoxide), promoters (formic acid, acetic acid), catalysts (phosphotungstic acid, ferrous(II) sulfate, zirconium dioxide, vanadium pentoxide, aluminum oxide γ, copper(II) oxide), and phase transfer agents (isobutanol, tetraoctylammonium bromide, and tetra-*n*-butylammonium fluoride), were examined to identify the optimal combination for reducing sulfurous compounds in the UAOD process. The influence of the extraction stage and reactor vessel material on the desulfurization efficiency was also investigated. Results revealed that hydrogen peroxide, formic acid, phosphotungstic acid, and isobutyl alcohol were the most effective oxidizers, promoters, catalysts, and phase transfer agents, respectively. Response surface methodology was used to determine the optimal conditions by evaluating different concentrations of these reagents within specific ranges. The study considered ranges such as 10−70 vol % of hydrogen peroxide, 5−70 vol % of formic acid, 1−30 wt % of phosphotungstic acid, 1−30 vol % of isobutanol, and 5−40 min of ultrasonic ripple time. Empirical models were developed for each sulfurous compound type, providing optimal conditions for sulfur removal with an error margin of less than 0.1%. The validity of the suggested models was confirmed through an industrial data analysis. Additionally, it was observed that increasing the number of extraction stages improved desulfurization efficiency, and using a stainless-steel reactor vessel was more suitable than using a glass vessel.

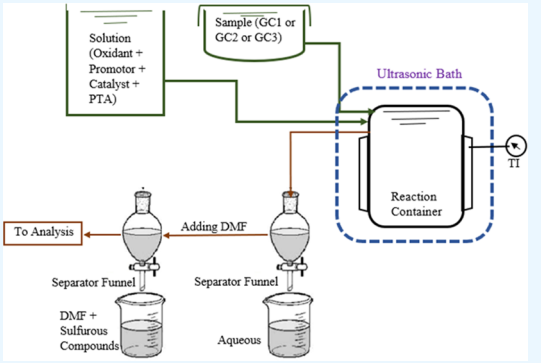

1. INTRODUCTION

Gas wells often produce natural gas and gas condensate, which commonly contain sulfurous compounds at levels that exceed acceptable thresholds for industrial use and other applications. Sulfur compounds in petroleum feedstocks contribute to environmental pollution and can harm the performance of engines and emission control systems.[1] Therefore, developing effective desulfurization methods is crucial to comply with increasingly stringent environmental regulations and improve the quality of refined fuels.

Various desulfurization methods have been proposed, including hydrodesulfurization (HDS), deep hydrodesulfurization (deep HDS), biodesulfurization, oxidative desulfurization (ODS), and ultrasound-assisted ODS (UAOD). HDS, the most commonly used method, is expensive and ineffective at removing aromatic sulfurous compounds. Modifications to HDS, such as using more active catalysts, longer reaction times, and higher temperatures (>400 °C) and pressures (>1000 atm), yield only marginal improvements in aromatic sulfurous compound removal. This process requires high temperatures and pressures, metallic catalysts, and extended reaction times.[2,3] Furthermore, this necessitates the establishment of a hydrogen production plant due to excessive hydrogen consumption. HDS is also associated with reduced removal efficiency, a significant increase in strongly aromatic sulfurous compounds, a shorter catalyst life span, and elevated operational costs.[4] Biodesulfurization processes are conducted at low temperatures and pressures with the assistance of microorganisms to degrade sulfurous compounds in crude oil.[5] However, this approach lacks mature technology, stable reactions, and reasonable reaction times.[6] ODS involves a chemical reaction between an oxidant and sulfur, eliminating the need for high pressures or temperatures.[7] While ODS can oxidize sulfurous compounds, it suffers from drawbacks such as the quantitative and qualitative reduction of fuel due to

Received: July 19, 2023
Revised: October 13, 2023
Accepted: October 19, 2023
Published: October 31, 2023

Table 1. Effect of the Solvent Type and Oxidant Mixture on the UAOD Efficiency

operating condition	feedstock	oxidant mixture	solvent	type and content of sulfurous compounds	removal efficiency (%)	refs
75 °C, 3 rounds of extraction for different times	diesel oil	tetradactyl ammonium bromide + phosphotungstic acid + hydrogen peroxide	acetonitrile	various types and contents	98.5	Mei et al.[23]
70 °C with ultrasonication for 10 min	diesel fuel	hydrogen peroxide + acetic acid + iron sulfide	acetonitrile	various types and contents	98	Ibrahim et al.[24]
50 °C, 4 rounds of extraction for 3 h	model diesel	cadmium oxide catalyst + hydrogen peroxide + acetic acid	acetonitrile	various types and contents	99.5	Zhao et al.[25]
ultrasonication for 10 min	kerosene	formic acid + hydrogen peroxide	acetonitrile	various types and contents	95	Babushkina et al.[26]
ultrasonication for 76 min and 4 rounds of extraction	kerosene	phosphotungstic acid supported on active carbon + hydrogen peroxide	acetonitrile	various types and contents	99	Gildo et al.[27]
70 °C	model diesel fuel	hydrogen peroxide + acetic acid	*N*, *N*-dimethylformamide	dibenzothiophene	98	Margeta et al.[28]
40 °C with ultrasonication for 15 min	diesel fuel	hydrogen peroxide + acetic acid + iron sulfide	*N*, *N*-dimethylformamide	dibenzothiophene	98	Dai et al.[29]
62 °C with ultrasonication for 17 min and 3 rounds of extraction	gasoil	hydrogen peroxide + acetic acid + iron sulfide + isobutanol	methanol	dibenzothiophene	90	Shayegan et al.[17]
90 °C with ultrasonication for 9 min and 3 rounds of extraction	diesel oil	hydrogen peroxide + acetic acid	methanol	dibenzothiophene	80	Duarte et al.[30]
50 °C	diesel oil	hydrogen peroxide + acetic acid + phosphotungstic acid + tetradactyl ammonium bromide	sodium hydroxide	dibenzothiophene	86	Shamseddini et al.[31]

https://doi.org/10.1021/acsomega.3c05193
ACS Omega 2023, 8, 42522−42539

oxidants and the loss of valuable fuel components if an inappropriate solvent is chosen.[8] To address the limitations of conventional desulfurization methods, the ultrasound-assisted oxidative desulfurization process (UAOD) has emerged as an innovative approach with several advantages. UAOD is a novel method that offers a quicker, safer, and more cost-effective oxidation process. It can efficiently remove both aliphatic and aromatic sulfurous compounds under low-pressure and low-temperature conditions, achieving a high yield of sulfur-to-sulfone conversion. It features short reaction times and is free from chemical hazards or the production of hazardous byproducts.[1,9] Additionally, UAOD is characterized by the use of recyclable catalysts.[1,9]

The UAOD process involves adding an oxidizing agent such as hydrogen peroxide (H_2O_2) to a sulfur-containing petroleum fraction, followed by exposure to ultrasonic irradiation. This generates reactive species, such as hydroxyl radicals ($^{\bullet}OH$), that are capable of oxidizing sulfur compounds. The oxidized sulfur species can then be separated from the desulfurized petroleum fraction using conventional techniques, such as extraction or distillation. UAOD offers advantages such as milder operating conditions compared to those of conventional methods, shorter reaction times, enhanced selectivity for sulfur compounds, and reduced catalyst usage. Importantly, UAOD can be seamlessly integrated into existing refining processes with minimal modifications, making it an appealing choice for the petroleum industry

Several studies have explored the effectiveness of the UAOD process in desulfurizing various petroleum fractions. Pouladi et al.[10] employed sulfuric acid (H_2SO_4), nitric acid (HNO_3), and nitrogen dioxide (NO_2) as oxidizing agents to optimize gas condensate desulfurization, achieving a remarkable sulfur removal efficiency of 95.61%. Alibolandi et al.[11] utilized ozone gas as an oxidizer to model and optimize gas condensate desulfurization, successfully removing 95.8% of sulfurous compounds under optimal conditions. In another study, Sinhmar et al.[12] achieved complete removal of sulfurous compounds from simulated diesel, including dibenzothiophene, using a combination of oxidizing agents (hydrogen peroxide, acetic acid, and potassium persulfate) in the UAOD process. Mofidi and Shahhosseini[13] employed a deep eutectic solvent (DES) in the UAOD process to remove dibenzothiophene (DBT) from diesel fuel, resulting in the removal of 97.53% of sulfurous compounds under optimal conditions. Desai et al.[14] applied the UAOD method to eliminate sulfurous compounds from model fuel (MF) containing DBT, achieving an impressive 99% removal rate. Fan et al.[15] introduced the Mo/Ti-TUD-1 catalyst in the UAOD method, achieving a 99% efficiency on a model oil and a 55.1% sulfurous removal rate for Saudi superlight oil. Additionally, Yu et al.[16] utilized a mixture of hydrogen peroxide, acetic acid, and copper(II) sulfate ($CuSO_4$) as an oxidizing agent and achieved a 48.68 wt % reduction in sulfur content from a heavy crude oil of Iran with a sulfurous content of 38,638 ppm. These studies collectively validate the effectiveness of the UAOD process in desulfurizing gas condensates. However, it is important to note that despite ongoing research on UAOD for sulfur removal from gas condensates, there remains a need for comprehensive investigations in this area. Most existing research has primarily focused on light or heavy oil samples, with limited attention given to the simultaneous removal of all sulfur compounds in the gas condensate, including aliphatic thiol, aliphatic sulfide, and aromatic thiophene.

Shayegan et al.[17] highlighted that the ultrasound-assisted oxidative desulfurization (UAOD) process inherently generates heat without the need for an external heat source. In their study investigating the temperature effect on desulfurization of sulfurous components from gas oil, the researchers explored a temperature range of 20 to 90 °C, with the upper limit set as the boiling point of the most volatile component in the mixture.[18−20] However, two key limitations emerged with increasing temperature: (1) the degradation of hydrogen peroxide at high temperatures, specifically above 80 °C, and (2) the evaporation of lighter gas oil components. Additionally, as the temperature increased, the effective creation of cavitation and the intensity of the cavitation collapse decreased. Consequently, to address these constraints, the researchers maintained a constant temperature of approximately 35 ± 2 °C throughout their experiments.[21,22] As a result, all experiments in this study were conducted at 35 ± 2 °C, ensuring the feasibility of the UAOD process while avoiding temperature-related issues.

In desulfurization, choosing materials, including oxidizers, promoters, catalysts, and phase transfer agents, is paramount to achieving efficient sulfur removal from hydrocarbon feedstocks. Their well-established utility and effectiveness often guide the selection of these materials in prior desulfurization studies conducted by researchers worldwide. Oxidizers such as hydrogen peroxide, sodium peroxide, and potassium superoxide have been extensively utilized due to their strong oxidizing properties, which facilitate the conversion of sulfur compounds into more readily removable forms. Promoters such as formic and acetic acids are commonly employed to enhance the desulfurization process by facilitating the action of oxidizers and catalysts. Catalysts, including phosphotungstic acid, ferrous(II) sulfate, zirconium dioxide, vanadium pentoxide, aluminum oxide γ, and copper(II) oxide, have played pivotal roles in desulfurization reactions by promoting the breakdown of complex sulfur compounds and aiding in their extraction. Phase transfer agents like isobutanol, tetraoctylammonium bromide, and tetra-*n*-butylammonium fluoride have been instrumental in transferring sulfur species from the hydrocarbon phase to the aqueous phase, further enhancing sulfur removal efficiency. These materials have a well-established track record in the desulfurization literature, with numerous studies showcasing their effectiveness in reducing the sulfur content in various hydrocarbon matrices. Table 1 reviews previous studies conducted on UAOD, highlighting the importance of solvent and oxidizing mixture selection. By leveraging the knowledge accumulated from prior research, this study has strategically chosen these materials as the basis for experimental investigations, aiming to contribute to ongoing efforts to develop more efficient and environmentally friendly desulfurization processes.

The primary objective of this study was to utilize the UAOD process for the degradation of linear and cyclic sulfur compounds found in synthetic gas condensates. Three specific sulfurous compounds were chosen, namely, *tert*-butyl mercaptan representing aliphatic thiol, dipropyl sulfide representing aliphatic sulfide, and benzothiophene representing aromatic thiophene. These compounds were initially present in concentrations ranging from 100 to 3000 ppm in *n*-heptane. To enhance the performance of the UAOD process, an oxidizer mixture comprising an oxidant, promoter, catalyst, and phase transfer agent was employed. Numerous oxidizers, promoters, catalysts, and phase transfer agents were tested

https://doi.org/10.1021/acsomega.3c05193
ACS Omega 2023, 8, 42522−42539

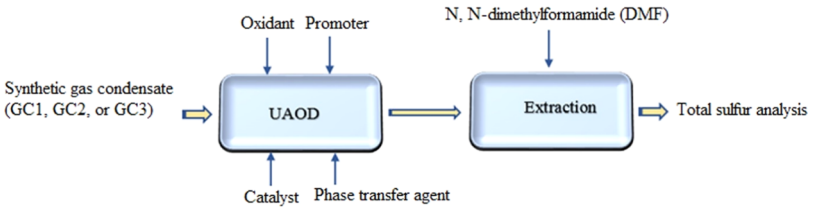

Figure 1. Schematic diagram of the UAOD process of sulfurous compounds removal in samples: GC_1, GC_2, and GC_3.

Table 2. Experimental Results to Obtain the Optimal Combination of the Oxidizer Mixture

			oxidizer blend			
run	synthetic samples (100 mL)	initial concentration of sulfur (ppm)	oxidant (40 mol %)	promoter (37.5 mol %)	catalyst (15.5 wt %)	SRE (%)
1	CG_1	3000	hydrogen peroxide			43.42
2	CG_1	3000	sodium peroxide			31.21
3	CG_1	3000	potassium superoxide			43.01
4	CG_2	3000	hydrogen peroxide			35.71
5	CG_2	3000	sodium peroxide			27.91
6	CG_2	3000	potassium superoxide			32.02
7	CG_3	3000	hydrogen peroxide			36.51
8	CG_3	3000	sodium peroxide			29.71
9	CG_3	3000	potassium superoxide			32.01
10	CG_1	3000	hydrogen peroxide	formic acid		77.96
11	CG_1	3000	hydrogen peroxide	acetic acid		76.02
12	CG_2	3000	hydrogen peroxide	formic acid		68.57
13	CG_2	3000	hydrogen peroxide	acetic acid		66.97
14	CG_3	3000	hydrogen peroxide	formic acid		61.73
15	CG_3	3000	hydrogen peroxide	acetic acid		60.87
16	CG_1	3000	hydrogen peroxide	formic acid	phosphotungstic acid	98.31
17	CG_1	3000	hydrogen peroxide	formic acid	ferrous(II) sulfate	97.12
18	CG_1	3000	hydrogen peroxide	formic acid	zirconium dioxide	80.47
19	CG_1	3000	hydrogen peroxide	formic acid	vanadium pentoxide	87.96
20	CG_1	3000	hydrogen peroxide	formic acid	aluminum oxide γ	93.56
21	CG_1	3000	hydrogen peroxide	formic acid	copper(II) oxid	95.26
22	CG_2	3000	hydrogen peroxide	formic acid	phosphotungstic acid	97.02
23	CG_2	3000	hydrogen peroxide	formic acid	ferrous(II) sulfate	96.21
24	CG_2	3000	hydrogen peroxide	formic acid	zirconium dioxide	68.08
25	CG_2	3000	hydrogen peroxide	formic acid	vanadium pentoxide	83.05
26	CG_2	3000	hydrogen peroxide	formic acid	aluminum oxide γ	91.78
27	CG_2	3000	hydrogen peroxide	formic acid	copper(II) oxide	94.06
28	CG_3	3000	hydrogen peroxide	formic acid	phosphotungstic acid	97.21
29	CG_3	3000	hydrogen peroxide	formic acid	ferrous(II) sulfate	95.97
30	CG_3	3000	hydrogen peroxide	formic acid	zirconium dioxide	72.36
31	CG_3	3000	hydrogen peroxide	formic acid	vanadium pentoxide	83.31
32	CG_3	3000	hydrogen peroxide	formic acid	aluminum oxide γ	91.99
33	CG_3	3000	hydrogen peroxide	formic acid	copper(II) oxide	94.71
34	CG_1	3000	hydrogen peroxide	formic acid	phosphotungstic acid	99.96
35	CG_1	3000	hydrogen peroxide	formic acid	phosphotungstic acid	99.17
36	CG_1	3000	hydrogen peroxide	formic acid	phosphotungstic acid	98.61
37	CG_2	3000	hydrogen peroxide	formic acid	phosphotungstic acid	98.77
38	CG_2	3000	hydrogen peroxide	formic acid	phosphotungstic acid	98.51
39	CG_2	3000	hydrogen peroxide	formic acid	phosphotungstic acid	97.18
40	CG_3	3000	hydrogen peroxide	formic acid	phosphotungstic acid	99.84
41	CG_3	3000	hydrogen peroxide	formic acid	phosphotungstic acid	98.99
42	CG_3	3000	hydrogen peroxide	formic acid	phosphotungstic acid	97.53

individually, followed by a comprehensive exploration of different combinations to determine the most effective oxidizing mixture. Subsequently, empirical models were developed for each type of sulfurous compound to predict optimal conditions for sulfur removal. Notably, this study is pioneering, as it investigates a wide range of three distinct sulfur compounds simultaneously. It also examines various values and types of oxidizers, promoters, catalysts, and phase transfer agents to optimize the UAOD process. Besides, the impact of the extraction stage and reactor vessel material was examined on the desulfurization efficiency. This article introduces three valuable mathematical models that predict

https://doi.org/10.1021/acsomega.3c05193
ACS Omega 2023, 8, 42522−42539

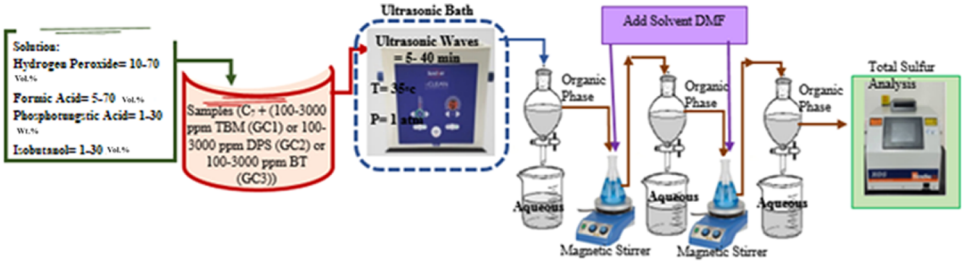

Figure 2. Schematic diagram illustrating the steps of the experiment created by Ameneh Taghizadeh.

sulfur removal efficiency for *tert*-butyl mercaptan, dipropyl sulfide, and benzothiophene. Finally, the validity of the suggested models was confirmed by using industrial data.

2. EXPERIMENTAL SECTION

2.1. Materials and Instruments. All of the chemicals used in this study were obtained from Merck and used without further purification. The chemicals include formic acid (CH_2O_2, 99%), acetic acid ($C_2H_4O_2$, 99%), hydrogen peroxide (H_2O_2, 30%), sodium peroxide (Na_2O_2, 99%), potassium superoxide (K_2O, 98%), phosphotungstic acid ($H_3P(W_3O_{10})_4$, 97%), ferrous(II) sulfate ($FeSO_4$, 99.5%), zirconium dioxide (ZrO_2, 99.99%), vanadium pentoxide (V_2O_5, ≥99.6%), aluminum oxide γ (Al_2O_3, 99.99%), copper(II) oxide (CuO, ≥99.0%), isobutanol ($C_4H_{10}O$, 99%), tetraoctylammonium bromide ($C_{32}H_{68}BrN$, 98%), tetra-*n*-butylammonium fluoride ($C_{16}H_{36}FN$, 98%), *n*-heptane (C_7H_{16}, 99%), *tert*-butyl mercaptan ($C_4H_{10}S$, 98%), dipropyl sulfide ($C_6H_{14}S$, 98%), benzothiophene (C_8H_6S, 98%), and *N*,*N*-dimethylformamide (DMF) ($HCON(CH_3)_2$, 99.8%). An XOS TSA (total sulfur analyzer) manufactured in the U.S.A. was used to analyze the sulfur levels in the gas-condensate samples. The TSA used in this research adheres to the ASTMD 7039 methodology, specifically designed to analyze gas-condensate samples.

2.2. Experimental Setup. An ultrasonic bath apparatus manufactured in Iran (VCLEAN 1-L6) was employed to conduct the experiments. This apparatus boasted adjustable temperature and water circulation capabilities and operated at 150 W and 40 kHz frequency. It also had a 6 L capacity and was used to sonicate the samples in two cylindrical vessels: the first reactor was made of SS-304 with a volume of 100 mL, and the second reactor was a Pyrex beaker with the same volume. Additionally, a hot plate with a magnetic stirrer manufactured by the IKA company (Yellow Line, model MSH basic, Germany) was used at a setting of 2000 rpm. To weigh the samples and take measurements, a laboratory precision balance (Sartorius PRACTUM 224−1S, Germany) with a precision of 0.1 mg and a sampler with an accuracy of 0.01 ppm were used. The steps for conducting the experiments are illustrated in Figure 1.

2.3. Experimental Procedure. In this study, gas-condensate systems contained two groups of sulfurous compounds: aliphatic species, such as thiols (mercaptans), and sulfides, as well as aromatic species, such as thiophene, benzothiophene, and dibenzothiophene. Generally, three representative samples were designated to examine the removal of each group of sulfurous compounds. The first group, represented by GC_1, consisted of *N*-heptane with the addition of *tert*-butyl mercaptan or 2-methyl-2-propane thiol, in the range 100−3000 ppm, to represent aliphatic thiols. The second group, represented by GC_2, consisted of *N*-heptane with the addition of dipropyl sulfide, in the range 100−3000 ppm, to represent aliphatic sulfides. Lastly, GC_3 consisted of *N*-heptane with benzothiophene, representing aromatic thiophenes in the 100−3000 ppm range.

To achieve the most effective oxidizer mixture, a variety of compounds were utilized, including hydrogen peroxide, sodium peroxide, and potassium superoxide as the oxidizer; formic acid and acetic acid as the promoter; phosphotungstic acid, ferrous(II) sulfate, zirconium dioxide, vanadium pentoxide, aluminum oxide γ, and copper(II) oxide as the catalyst; and isobutanol, tetraoctylammonium bromide, and tetra-*n*-butylammonium fluoride as the phase transfer agent. These compounds were combined in various ways, as outlined in Table 2. Three separate mixtures were created to prepare the samples, each containing a consistent sulfur content of 3000 ppm of distinct sulfurous compounds. The oxidizer mixture was then added to each of the samples. After this, the samples were sonicated for 22 min in an ultrasonic bath whose temperature was kept constant at 35 ± 2 °C by a PID controller. Following the predetermined ultrasonication time, the samples were removed from the bath and allowed to rest for 10 min. The resulting mixture was then divided into an organic phase on top and an aqueous phase at the bottom. The organic phase was separated and mixed twice with 10 mL of DMF (equivalent to half the volume of the hydrocarbon sample) as the extractor and agitated for 10 min by a magnetic stirrer at 300 rpm. After each extraction, the organic phase became clearer, eventually appearing like the original *n*-heptane as oxidized sulfurous compounds were efficiently removed. Finally, the organic phase sample was collected for total sulfur analysis, and the sulfur removal efficiency (SRE%) was calculated using eq 1. Figure 2 shows the steps of the experiment.

$$\text{SRE\%} = \frac{\text{initial sulfur content} - \text{final sulfur content}}{\text{initial sulfur content}} \times 100 \quad (1)$$

2.4. Experimental Design. To execute the Central Composite Design (CCD) with an α of 2, six variables, and five levels coded as (−2), (−1), (0), (+1), and (+2) according to eq 2, Design Expert Version 13 software was utilized.

$$N = 2^K + 2K + n_c \quad (2)$$

where, N is the total number of experiments, denoted by the CCD, and K considers the number of variables. Additionally, n_c represents the central points. Based on eq 2, the design involved 64 factorial points, 12 axial points, and 10 central points, resulting in 86 experiments for each gas-condensate sample, namely, GC_1, GC_2, and GC_3. Thus, the overall number of experiments required was 258.

https://doi.org/10.1021/acsomega.3c05193
ACS Omega 2023, 8, 42522−42539

2.5. Optimization. By employing numerical optimization, experiments can be focused on achieving a particular objective. In contrast to previous studies that solely concentrated on the sulfur content of specific wells, this study permits the estimation of the desulfurization efficiency under particular conditions. The current research offers insights into the ideal conditions for varying sulfur content levels, facilitating the anticipation of the desulfurization efficiency in optimal scenarios. To validate the optimal conditions, conducting the confirmed experiments recommended by CCD becomes essential. The confirmed experiments were executed according to the optimum conditions.

2.6. Effect of Extraction Stage and Reactor Vessel Material. This study investigated the impact of the extraction stage and reactor vessel material on the desulfurization efficiency. To achieve this, a polar solvent called DMF was utilized for extraction using a solvent-to-hydrocarbon ratio of 2:1. Subsequently, experiments were carried out at the optimal points determined for GC_1, GC_2, and GC_3. Each sample underwent three different experiments. First, two extraction stages were conducted using a glass reactor vessel. Second, two extraction stages were performed using a stainless-steel reactor vessel. Lastly, three extraction stages were executed using the most suitable reactor vessel type, either glass or stainless steel.

2.7. Field Data. After successfully removing mercaptan from the GC_1 with a desulfurization efficiency of 99.93% using UAOP under optimal conditions, a comparison was conducted between two industrial gas-condensate samples containing mercaptan compounds before and after the H_2S polishing process. These samples were obtained from the Fifth Gas Refinery, Phases 10 and 11 of the South Pars Complex, Iran, and their respective characteristics are listed in Tables 2 and 3.

Table 3. Compositions of Gas Condensates, Prepared from the Fifth Gas Refinery, Phases 10 and 11 of the South Pars Complex, Iran

property	method	industrial sample 1 (ppm)	industrial sample 2 (ppm)
Sp. Gr. 60/60 °F	ASTM D4052	0.740	0.732
total sulfur	ASTM D7039	1726.30	1521.87
mercaptans	ASTM D3227	2400	2243
H_2S	ASTM D1159	20	5

The total sulfur contents of the industrial samples (IS_1 and IS_2) were measured at 1726.30 and 1521.87 ppm, respectively. The optimal operating conditions were extracted using Design Expert software, and a constant value of X_1 was entered in the optimization section for the first model. This resulted in the determination of the optimal points for removing the specified amount of sulfur from both industrial samples.

3. RESULTS AND DISCUSSION

3.1. Optimizing the Type and Magnitude of the Variables. In this study, initially, 42 different experiments were accomplished to find the best types of oxidizer, promoter, catalyst, and phase transfer agent. According to the findings presented in Table 4, the optimal selections for oxidizers, promoters, catalysts, and phase transfer agents were hydrogen peroxide, formic acid, phosphotungstic acid, and isobutanol, in that order.

After determining the best type of oxidizer, promoter, catalyst, and phase transfer agent, optimizing these parameters based on the CCD method was tried. Table 5 displays the experiments suggested by the experimental design and the obtained results, outlining the independent variables under consideration in this study. These variables comprise the sulfur content for each of GC_1, GC_2, and GC_3 (X_1), the oxidant (10−70 vol % of hydrogen peroxide) (X_2), the enhancer (5−70 vol % of formic acid) (X_3), the catalyst (1−30 wt % of phosphotungstic acid) (X_4), the phase transfer agent dosage (1−30 vol % of isobutanol) (X_5), and the ultrasonic time (5−40 min) (X_6). In addition, certain factors remained constant throughout the research, such as the sonication power of 150 W, the sonication frequency of 40 kHz, and the stirring of a magnetic stirrer at 300 rpm. The ultrasonic bath temperature was maintained at 35 ± 2 °C under atmospheric pressure for 10 min in each extraction round.

Table 6 displays the results of the analysis of variances (ANOVA), where the combination of high F-statistics and small p-values indicates both the validity of the models and the significance of the coefficients in the built models. For the three gas-condensate samples, variables with p-values less than 0.05 substantially impact the response and, therefore, cannot be disregarded. Additionally, the table reveals exceptional correlation coefficients (R^2) for all three models, which measure the relationship between the response and independent variables and their interactions. In essence, R^2 serves as an indicator of how closely the model predictions resemble the experimental data. The minor differences between the adjusted correlation coefficient (R_{Adj}^2) and the predicted correlation coefficient (R_{Pred}^2) for all three samples demonstrate the reliability of the mathematical model presented.

3.2. Introducing the Mathematical Models. Drawing from the CCD, eq 3 can be utilized to articulate the quadratic association linking the response and variables

$$Y_{SER\%} = \alpha_0 + \sum_{i=1}^{6} \alpha_i X_i + \sum_{i=1}^{6} \sum_{j=i+1}^{6} \alpha_{ij} X_i X_j + \sum_{i=1}^{6} \alpha_{ii} X_i^2 + \varepsilon \quad (3)$$

The equation comprises various components, including the response variable for sulfur removal efficiency denoted as $Y_{SER\%}$. The parameters X_1,..., and X_i are coded parameters, while α_0 is the interception term, and α_1,..., α_i represent the regression coefficients for linear effects. Furthermore, α_{ii} corresponds to the regression coefficients for squared effects, α_{ij} is the regression coefficient for interaction effects, and ε denotes the error component.

Using the encoded values of various variables presented in Table 6, a quadratic form for each of the three samples was expressed in eqs 45−6.

$$\begin{aligned} Y_{SER\%(CG_1)} = {} & 99.13 + 0.1554X_1 - 0.1440X_2 + 0.1318X_3 \\ & + 0.499X_4 + 0.0621X_5 + 0.0986X_1X_2 \\ & - 0.0698X_1X_3 - 0.0595X_1X_6 + 0.0739X_2X_3 \\ & + 0.1021X_1^2 + 0.1096X_2^2 + 0.0771X_3^2 \\ & + 0.0958X_4^2 + 0.0571X_5^2 + 0.1333X_6^2 \end{aligned} \quad (4)$$

https://doi.org/10.1021/acsomega.3c05193
ACS Omega 2023, 8, 42522−42539

Table 4. Experimental Results for the Removal of Mercaptan (SRE%(CG_1)), Sulfide (SRE%(CG_2)), and Thiophene Compound (SRE%(CG_3)) by UAOD Method from the Three-Sample Synthetic Gas Condensate with the Help of RSM Based on CCD

	variables												SRE (%)		
	X_1		X_2		X_3		X_4		X_5		X_6				
run	ppm	code	vol %	code	vol %	code	wt %	code	vol %	code	min	code	GC_1	GC_2	GC_3
1	825	−1	25	−1	21.3	−1	8.3	−1	8.3	−1	13.8	−1	99.59	96.11	86.13
2	2275	1	25	−1	21.3	−1	8.3	−1	8.3	−1	13.8	−1	99.88	97.93	98.31
3	825	−1	55	1	21.3	−1	8.3	−1	8.3	−1	13.8	−1	98.58	94.45	82.41
4	2275	1	55	1	21.3	−1	8.3	−1	8.3	−1	13.8	−1	99.85	96.12	97.73
5	825	−1	25	−1	53.8	1	8.3	−1	8.3	−1	13.8	−1	99.78	96.78	87.46
6	2275	1	25	−1	53.8	1	8.3	−1	8.3	−1	13.8	−1	99.90	98.41	98.62
7	825	−1	55	1	53.8	1	8.3	−1	8.3	−1	13.8	−1	99.47	95.48	84.21
8	2275	1	55	1	53.8	1	8.3	−1	8.3	−1	13.8	−1	99.86	97.14	97.97
9	825	−1	25	−1	21.3	−1	22.8	1	8.3	−1	13.8	−1	99.68	96.42	89.23
10	2275	1	25	−1	21.3	−1	22.8	1	8.3	−1	13.8	−1	99.91	98.15	98.47
11	825	−1	55	1	21.3	−1	22.8	1	8.3	−1	13.8	−1	98.75	95.16	86.96
12	2275	1	55	1	21.3	−1	22.8	1	8.3	−1	13.8	−1	99.87	96.69	98.13
13	825	−1	25	−1	53.8	1	22.8	1	8.3	−1	13.8	−1	99.92	97.23	90.13
14	2275	1	25	−1	53.8	1	22.8	1	8.3	−1	13.8	−1	99.96	98.86	98.96
15	825	−1	55	1	53.8	1	22.8	1	8.3	−1	13.8	−1	99.49	95.97	88.63
16	2275	1	55	1	53.8	1	22.8	1	8.3	−1	13.8	−1	99.89	97.77	98.26
17	825	−1	25	−1	21.3	−1	8.3	−1	22.8	1	13.8	−1	99.73	96.83	94.12
18	2275	1	25	−1	21.3	−1	8.3	−1	22.8	1	13.8	−1	99.92	98.31	99.36
19	825	−1	55	1	21.3	−1	8.3	−1	22.8	1	13.8	−1	98.85	95.29	89.13
20	2275	1	55	1	21.3	−1	8.3	−1	22.8	1	13.8	−1	99.89	97.07	99.01
21	825	−1	25	−1	53.8	1	8.3	−1	22.8	1	13.8	−1	99.93	97.98	95.09
22	2275	1	25	−1	53.8	1	8.3	−1	22.8	1	13.8	−1	99.97	99.13	99.45
23	825	−1	55	1	53.8	1	8.3	−1	22.8	1	13.8	−1	99.51	96.73	91.98
24	2275	1	55	1	53.8	1	8.3	−1	22.8	1	13.8	−1	99.90	97.98	99.19
25	825	−1	25	−1	21.3	−1	22.8	1	22.8	1	13.8	−1	99.86	98.02	95.08
26	2275	1	25	−1	21.3	−1	22.8	1	22.8	1	13.8	−1	99.97	99.09	99.46
27	825	−1	55	1	21.3	−1	22.8	1	22.8	1	13.8	−1	99.13	96.31	92.73
28	2275	1	55	1	21.3	−1	22.8	1	22.8	1	13.8	−1	99.94	97.92	99.21
29	825	−1	25	−1	53.8	1	22.8	1	22.8	1	13.8	−1	99.95	98.83	96.56
30	2275	1	25	−1	53.8	1	22.8	1	22.8	1	13.8	−1	99.99	99.55	99.59
31	825	−1	55	1	53.8	1	22.8	1	22.8	1	13.8	−1	99.70	97.64	93.16
32	2275	1	55	1	53.8	1	22.8	1	22.8	1	13.8	−1	99.95	98.56	99.43
33	825	−1	25	−1	21.3	−1	8.3	−1	8.3	−1	31.3	1	99.65	96.87	90.72
34	2275	1	25	−1	21.3	−1	8.3	−1	8.3	−1	31.3	1	99.83	97.73	96.41
35	825	−1	55	1	21.3	−1	8.3	−1	8.3	−1	31.3	1	98.90	95.31	87.12
36	2275	1	55	1	21.3	−1	8.3	−1	8.3	−1	31.3	1	99.31	95.91	94.16
37	825	−1	25	−1	53.8	1	8.3	−1	8.3	−1	31.3	1	99.80	97.58	91.52
38	2275	1	25	−1	53.8	1	8.3	−1	8.3	−1	31.3	1	99.85	98.03	97.02
39	825	−1	55	1	53.8	1	8.3	−1	8.3	−1	31.3	1	99.58	95.91	88.96
40	2275	1	55	1	53.8	1	8.3	−1	8.3	−1	31.3	1	99.83	96.59	95.71
41	825	−1	25	−1	21.3	−1	22.8	1	8.3	−1	31.3	1	99.72	97.10	94.31
42	2275	1	25	−1	21.3	−1	22.8	1	8.3	−1	31.3	1	99.87	97.96	98.14
43	825	−1	55	1	21.3	−1	22.8	1	8.3	−1	31.3	1	99.05	95.97	89.21
44	2275	1	55	1	21.3	−1	22.8	1	8.3	−1	31.3	1	99.42	96.31	97.71
45	825	−1	25	−1	53.8	1	22.8	1	8.3	−1	31.3	1	99.93	97.73	95.89
46	2275	1	25	−1	53.8	1	22.8	1	8.3	−1	31.3	1	99.94	98.33	98.73
47	825	−1	55	1	53.8	1	22.8	1	8.3	−1	31.3	1	99.65	96.59	92.13
48	2275	1	55	1	53.8	1	22.8	1	8.3	−1	31.3	1	99.84	97.03	97.95
49	825	−1	25	−1	21.3	−1	8.3	−1	22.8	1	31.3	1	99.78	97.53	95.89
50	2275	1	25	−1	21.3	−1	8.3	−1	22.8	1	31.3	1	99.91	98.13	99.06
51	825	−1	55	1	21.3	−1	8.3	−1	22.8	1	31.3	1	99.16	96.06	92.33
52	2275	1	55	1	21.3	−1	8.3	−1	22.8	1	31.3	1	99.55	96.91	98.19
53	825	−1	25	−1	53.8	1	8.3	−1	22.8	1	31.3	1	99.94	98.17	97.66
54	2275	1	25	−1	53.8	1	8.3	−1	22.8	1	31.3	1	99.96	98.89	99.22
55	825	−1	55	1	53.8	1	8.3	−1	22.8	1	31.3	1	99.62	96.93	93.18
56	2275	1	55	1	53.8	1	8.3	−1	22.8	1	31.3	1	99.86	97.65	98.67

https://doi.org/10.1021/acsomega.3c05193
ACS Omega 2023, 8, 42522−42539

Table 4. continued

	variables												SRE (%)		
	X_1		X_2		X_3		X_4		X_5		X_6				
run	ppm	code	vol %	code	vol %	code	wt %	code	vol %	code	min	code	GC_1	GC_2	GC_3
57	825	−1	25	−1	21.3	−1	22.8	1	22.8	1	31.3	1	99.88	98.47	97.72
58	2275	1	25	−1	21.3	−1	22.8	1	22.8	1	31.3	1	99.93	98.69	99.17
59	825	−1	55	1	21.3	−1	22.8	1	22.8	1	31.3	1	99.41	96.90	96.05
60	2275	1	55	1	21.3	−1	22.8	1	22.8	1	31.3	1	99.73	97.58	98.63
61	825	−1	25	−1	53.8	1	22.8	1	22.8	1	31.3	1	99.97	98.96	98.02
62	2275	1	25	−1	53.8	1	22.8	1	22.8	1	31.3	1	99.99	99.11	99.33
63	825	−1	55	1	53.8	1	22.8	1	22.8	1	31.3	1	99.75	97.85	96.89
64	2275	1	55	1	53.8	1	22.8	1	22.8	1	31.3	1	99.89	97.99	98.99
65	100	−2	40	0	37.5	0	15.5	0	15.5	0	22.5	0	99.19	96.32	89.31
66	3000	2	40	0	37.5	0	15.5	0	15.5	0	22.5	0	99.96	98.77	99.84
67	1550	0	10	−2	37.5	0	15.5	0	15.5	0	22.5	0	99.52	97.93	98.02
68	1550	0	70	2	37.5	0	15.5	0	15.5	0	22.5	0	99.69	96.62	94.98
69	1550	0	40	0	5.0	−2	15.5	0	15.5	0	22.5	0	99.12	96.55	92.27
70	1550	0	40	0	70.0	2	15.5	0	15.5	0	22.5	0	99.83	98.89	96.09
71	1550	0	40	0	37.5	0	1.0	−2	15.5	0	22.5	0	99.35	96.83	96.33
72	1550	0	40	0	37.5	0	30.0	2	15.5	0	22.5	0	99.75	98.06	99.22
73	1550	0	40	0	37.5	0	15.5	0	1.0	−2	22.5	0	99.27	96.38	93.07
74	1550	0	40	0	37.5	0	15.5	0	30.0	2	22.5	0	99.52	98.11	99.42
75	1550	0	40	0	37.5	0	15.5	0	15.5	0	5.0	−2	99.45	97.18	95.71
76	1550	0	40	0	37.5	0	15.5	0	15.5	0	40.0	2	99.95	98.66	98.21
77	1550	0	40	0	37.5	0	15.5	0	15.5	0	22.5	0	99.12	97.7	97.38
78	1550	0	40	0	37.5	0	15.5	0	15.5	0	22.5	0	99.14	97.72	97.38
79	1550	0	40	0	37.5	0	15.5	0	15.5	0	22.5	0	99.12	97.69	97.39
80	1550	0	40	0	37.5	0	15.5	0	15.5	0	22.5	0	99.12	97.69	97.39
81	1550	0	40	0	37.5	0	15.5	0	15.5	0	22.5	0	99.13	97.69	97.41
82	1550	0	40	0	37.5	0	15.5	0	15.5	0	22.5	0	99.1	97.67	97.39
83	1550	0	40	0	37.5	0	15.5	0	15.5	0	22.5	0	99.12	97.68	97.39
84	1550	0	40	0	37.5	0	15.5	0	15.5	0	22.5	0	99.11	97.69	97.39
85	1550	0	40	0	37.5	0	15.5	0	15.5	0	22.5	0	99.12	97.68	97.39
86	1550	0	40	0	37.5	0	15.5	0	15.5	0	22.5	0	99.12	97.69	97.39

$$Y_{SER\%(CG_2)} = 99.71 + 0.5175X_1 - 0.6356X_2 + 0.3994X_3 + 0.2953X_4 + 0.4847X_5 + 0.0808X_6 - 0.0663X_1X_5 - 0.2272X_1X_6 + 0.0566X_2X_3 - 0.0666X_3X_6 + 0.0775X_4X_5 - 0.1205X_2^2 - 0.0780X_4^2 - 0.1280X_5^2 \quad (5)$$

$$Y_{SER\%(CG_3)} = 99.44 + 3.18X_1 - 0.929X_2 + 0.4988X_3 + 0.8701X_4 + 1.76X_5 + 0.6324X_6 + 0.6264X_1X_2 - 0.2561X_1X_3 - 0.5111X_1X_4 - 1.05X_1X_5 - 1.07X_1X_6 + 0.1777X_2X_4 - 0.3108X_4X_5 - 0.747X_1^2 - 0.2657X_2^2 - 0.8457X_3^2 - 0.3295X_5^2 \quad (6)$$

3.3. Statistical Graphs. Figure 3(a_1,a_2,a_3) demonstrates the comparison between the model and empirical data, exhibiting a favorable level of agreement. On the other hand, Figure 3(b_1,b_2,b_3), which showcases the deviation model, allows for the comparison of the impacts of individual parameters on the model. In this regard, the variables' center points in Table 4 are designated as code 0. A pronounced incline implies a heightened level of sensitivity, whereas a comparatively gentle incline signifies a lack of sensitivity. Notably, the response was observed to be sensitive to all inputs.

3.4. UAOD Mechanism. UAOD is a process that utilizes both the aqueous and organic phases. In this particular study, the oxidants and enhancers used were hydrogen peroxide and formic acid, respectively. The catalyst used was phosphotungstic acid, also known as polyoxometalate acid, while isobutyl alcohol acted as a phase transfer agent. A competitive reaction takes place during catalytic oxidation in the aqueous phase involving two mechanisms. The first mechanism involves the reaction of formic acid with hydrogen peroxide, resulting in the formation of performic acid and subsequent decomposition to produce free radicals of *OOH. The second mechanism involves the reaction of hydrogen peroxide with phosphotungstic acid to produce proxy-poly(tungstate) anions. Depending on the components present in the aqueous phase, both mechanisms may occur simultaneously, as in this study, where both catalyst and promoter were used. Both mechanisms may occur simultaneously, and the relative dominance of each depends on the quantities of hydrogen peroxide, formic acid, and phosphotungstic acid used. Therefore, in this study, these parameters were optimized to harness the combined potential of both mechanisms, ultimately maximizing the sulfur removal efficiency. Mechanism (1) comprises eqs 7−10, in which the oxidant attacks the enhancer to oxidize and produce free radicals. As a result of the

https://doi.org/10.1021/acsomega.3c05193
ACS Omega 2023, 8, 42522−42539

Table 5. Analysis of Variance (ANOVA) for the RSM for Three Synthetic Gas Condensate Samples

		ANOVA					coefficient of quadratic equation in terms of coded factors		
source model	type	sum of squares	D_f	mean square	F-value	P-value	CG_1	GC_2	GC_3
	GC_1	9.69	27	0.3591	21.48	<0.0001 significant	+99.13		
	GC_2	90.51	27	3.35	66.48	<0.0001 significant		+97.71	
	GC_3	1382.21	27	51.19	108.29	<0.0001 significant			+97.44
X_1	GC_1	1.74	1	1.74	104.02	<0.0001	+0.1554		
	GC_2	19.28	1	19.28	382.39	<0.0001		+0.5175	
	GC_3	726.38	1	726.38	1536.58	<0.0001			+3.18
X_2	GC_1	1.49	1	1.49	89.33	<0.0001	−0.1440		
	GC_2	29.08	1	29.08	576.75	<0.0001		−0.6356	
	GC_3	62.14	1	62.14	131.46	<0.0001			−0.9290
X_3	GC_1	1.25	1	1.25	74.81	<0.0001	+0.1318		
	GC_2	11.49	1	11.49	227.82	<0.0001		+0.3994	
	GC_3	17.91	1	17.91	37.89	<0.0001			+0.4988
X_4	GC_1	0.1790	1	0.1790	10.70	0.0018	+0.0499		
	GC_2	6.28	1	6.28	124.49	<0.0001		+0.2953	
	GC_3	54.51	1	54.51	115.32	<0.0001			+0.8701
X_5	GC_1	0.2775	1	0.2775	16.58	0.0001	+0.0621		
	GC_2	16.92	1	16.92	335.48	<0.0001		+0.4847	
	GC_3	223.84	1	223.84	473.51	<0.0001			+1.76
X_6	GC_1	0.0120	1	0.0120	0.7177	0.4004	+0.0129		
	GC_2	0.4705	1	0.4705	9.33	0.0034		+0.0808	
	GC_3	28.79	1	28.79	60.91	<0.0001			+0.6324
X_1X_2	GC_1	0.6221	1	0.6221	37.17	<0.0001	+0.0986		
	GC_2	0.0150	1	0.0150	0.2976	0.5875		+0.0153	
	GC_3	25.11	1	25.11	53.12	<0.0001			+0.6264
X_1X_3	GC_1	0.3122	1	0.3122	18.65	<0.0001	−0.0698		
	GC_2	0.1444	1	0.1444	2.86	0.0960		−0.0475	
	GC_3	4.20	1	4.20	8.88	0.0042			−0.2561
X_1X_4	GC_1	0.0207	1	0.0207	1.23	0.2711	−0.0180		
	GC_2	0.1892	1	0.1892	3.75	0.0576		−0.0544	
	GC_3	16.72	1	16.72	35.37	<0.0001			−0.5111
X_1X_5	GC_1	0.0260	1	0.0260	1.55	0.2176	−0.0202		
	GC_2	0.2809	1	0.2809	5.57	0.0216		−0.0663	
	GC_3	69.91	1	69.91	147.89	<0.0001			−1.05
X_1X_6	GC_1	0.2268	1	0.2268	13.55	0.0005	−0.0595		
	GC_2	3.30	1	3.30	65.51	<0.0001		−0.2272	
	GC_3	73.64	1	73.64	155.77	<0.0001			−1.07
X_2X_3	GC_1	0.3496	1	0.3496	20.89	<0.0001	+0.0739		
	GC_2	0.2048	1	0.2048	4.06	0.0485		+0.0566	
	GC_3	0.3798	1	0.3798	0.8034	0.3738			+0.0770
X_2X_4	GC_1	0.0074	1	0.0074	0.4445	0.5076	+0.0108		
	GC_2	0.1073	1	0.1073	2.13	0.1501		+0.0409	
	GC_3	2.02	1	2.02	4.27	0.0432			+0.1777
X_2X_5	GC_1	0.0166	1	0.0166	0.9904	0.3238	+0.0161		
	GC_2	0.0977	1	0.0977	1.94	0.1693		+0.0391	
	GC_3	0.3585	1	0.3585	0.7584	0.3874			+0.0748
X_2X_6	GC_1	0.0001	1	0.0001	0.0076	0.9310	−0.0014		
	GC_2	0.0030	1	0.0030	0.0600	0.8074		−0.0069	
	GC_3	0.3985	1	0.3985	0.8429	0.3624			−0.0789
X_3X_4	GC_1	0.0074	1	0.0074	0.4445	0.5076	−0.0108		
	GC_2	0.0380	1	0.0380	0.7541	0.3888		−0.0244	
	GC_3	0.1796	1	0.1796	0.3799	0.5401			−0.0530
X_3X_5	GC_1	0.0395	1	0.0395	2.36	0.1299	−0.0248		
	GC_2	0.0400	1	0.0400	0.7932	0.3768		+0.0250	
	GC_3	0.5130	1	0.5130	1.09	0.3019			−0.0895
X_3X_6	GC_1	0.0044	1	0.0044	0.2622	0.6105	+0.0083		
	GC_2	0.2836	1	0.2836	5.62	0.0211		−0.0666	
	GC_3	0.0523	1	0.0523	0.1107	0.7406			+0.0286
X_4X_5	GC_1	0.0017	1	0.0017	0.1017	0.7510	+0.0052		
	GC_2	0.3844	1	0.3844	7.62	0.0077		+0.0775	

https://doi.org/10.1021/acsomega.3c05193
ACS Omega 2023, 8, 42522−42539

Table 5. continued

		ANOVA					coefficient of quadratic equation in terms of coded factors		
source model	type	sum of squares	D_f	mean square	F-value	P-value	CG_1	GC_2	GC_3
	GC_3	6.18	1	6.18	13.08	0.0006			−0.3108
X_4X_6	GC_1	0.0001	1	0.0001	0.0076	0.9310	+0.0014		
	GC_2	0.0663	1	0.0663	1.31	0.2562		−0.0322	
	GC_3	1.33	1	1.33	2.82	0.0987			+0.1442
X_5X_6	GC_1	0.0019	1	0.0019	0.1144	0.7364	+0.0055		
	GC_2	0.0452	1	0.0452	0.8955	0.3479		−0.0266	
	GC_3	0.9096	1	0.9096	1.92	0.1707			−0.1192
X_1^2	GC_1	0.3581	1	0.3581	21.39	<0.0001	+0.1021		
	GC_2	0.0970	1	0.0970	1.92	0.1707		−0.0530	
	GC_3	19.17	1	19.17	40.55	<0.0001			−0.7470
X_2^2	GC_1	0.4126	1	0.4126	24.65	<0.0001	+0.1096		
	GC_2	0.5001	1	0.5001	9.92	0.0026		−0.1205	
	GC_3	2.43	1	2.43	5.13	0.0272			−0.2657
X_3^2	GC_1	0.2042	1	0.2042	12.20	0.0009	+0.0771		
	GC_2	0.0030	1	0.0030	0.0602	0.8070		−0.0092	
	GC_3	24.57	1	24.57	51.98	<0.0001			−0.8457
X_4^2	GC_1	0.3156	1	0.3156	18.85	<0.0001	+0.0958		
	GC_2	0.2098	1	0.2098	4.16	0.0459		−0.0780	
	GC_3	0.0965	1	0.0965	0.2042	0.6530			+0.0530
X_5^2	GC_1	0.1120	1	0.1120	6.69	0.0122	+0.0571		
	GC_2	0.5642	1	0.5642	11.19	0.0014		−0.1280	
	GC_3	3.73	1	3.73	7.89	0.0068			−0.3295
X_6^2	GC_1	0.6108	1	0.6108	36.50	<0.0001	+0.1333		
	GC_2	0.0566	1	0.0566	1.12	0.2937		+0.0408	
	GC_3	0.7806	1	0.7806	1.65	0.2039			−0.1507
residual	GC_1	0.9707	58	0.0167					
	GC_2	2.92	58	0.0504					
	GC_3	27.42	58	0.4727					
lack of fit	GC_1	0.9697	49	0.0198	178.11	<0.0001			
	GC_2	2.92	49	0.0597	335.56	<0.0001			
	GC_3	27.42	49	0.5595	8393.06	<0.0001			
pure error	GC_1	0.0010	9	0.0001					
	GC_2	0.0016	9	0.0002					
	GC_3	0.0006	9	0.0001					
cor total	GC_1	10.67	85						
	GC_2	93.43	85						
	GC_3	1409.63	85						
fit statistics	GC_1	R^2 = 0.9090, adj-R^2= 0.8666, pred-R^2= 0.7319, model precision = 18.0658							
	GC_2	R^2 = 0.9687, adj-R^2= 0.9541, pred-R^2= 0.8994, model precision = 41.8028							
	GC_3	R^2 = 0.9805, adj-R^2= 0.9715, pred-R^2= 0.9510, model precision = 45.0703							

Table 6. Compassion of the Predicted and Experimental Results of the Three-Sample Synthetic Gas Condensate Containing Mercaptan, Sulfide, and Thiophene Compounds

sample		X_1 (ppm)	X_2 (vol %)	X_3 (vol %)	X_4 (wt %)	X_5 (vol %)	X_6 (min)	predicted R^2	experimental R^2
GC_1	actual	1357.60	48.05	69.72	8.96	5.60	11.33	100.0	99.93
	coded	−0.26	0.53	1.98	−0.90	−1.36	−1.27		
GC_2	actual	1618.14	12.54	67.66	27.95	18.93	5.83	99.71	99.63
	coded	0.09	−1.83	1.85	1.71	0.47	−1.90		
GC_3	actual	2972.64	30.08	27.83	5.04	22.91	20.22	100.0	99.81
	coded	1.96	−0.66	−0.59	−1.44	1.02	−0.26		

presence of these free radicals, sulfurous compounds are subsequently oxidized.

$$CHOOH + H_2O_2 \rightarrow CHOOOH + H_2O \quad (7)$$

$$CHOOOH \rightarrow CHO^{\bullet} + {}^{\bullet}OOH \quad (8)$$

$$RSR + {}^{\bullet}OOH \rightarrow R_2SO + {}^{\bullet}OH \quad (9)$$

$$^{\bullet}OH + CHO^{\bullet} \rightarrow CHOOH \quad (10)$$

According to Wan et al.,[32] the second mechanism involves the oxidation of sulfurous compounds upon attacking the catalyst with an oxidant. When there is an excess of hydrogen peroxide, phosphotungstic acid, acting as the catalyst, undergoes oxidation and becomes polyoxometalate acid. The

https://doi.org/10.1021/acsomega.3c05193
ACS Omega 2023, 8, 42522−42539

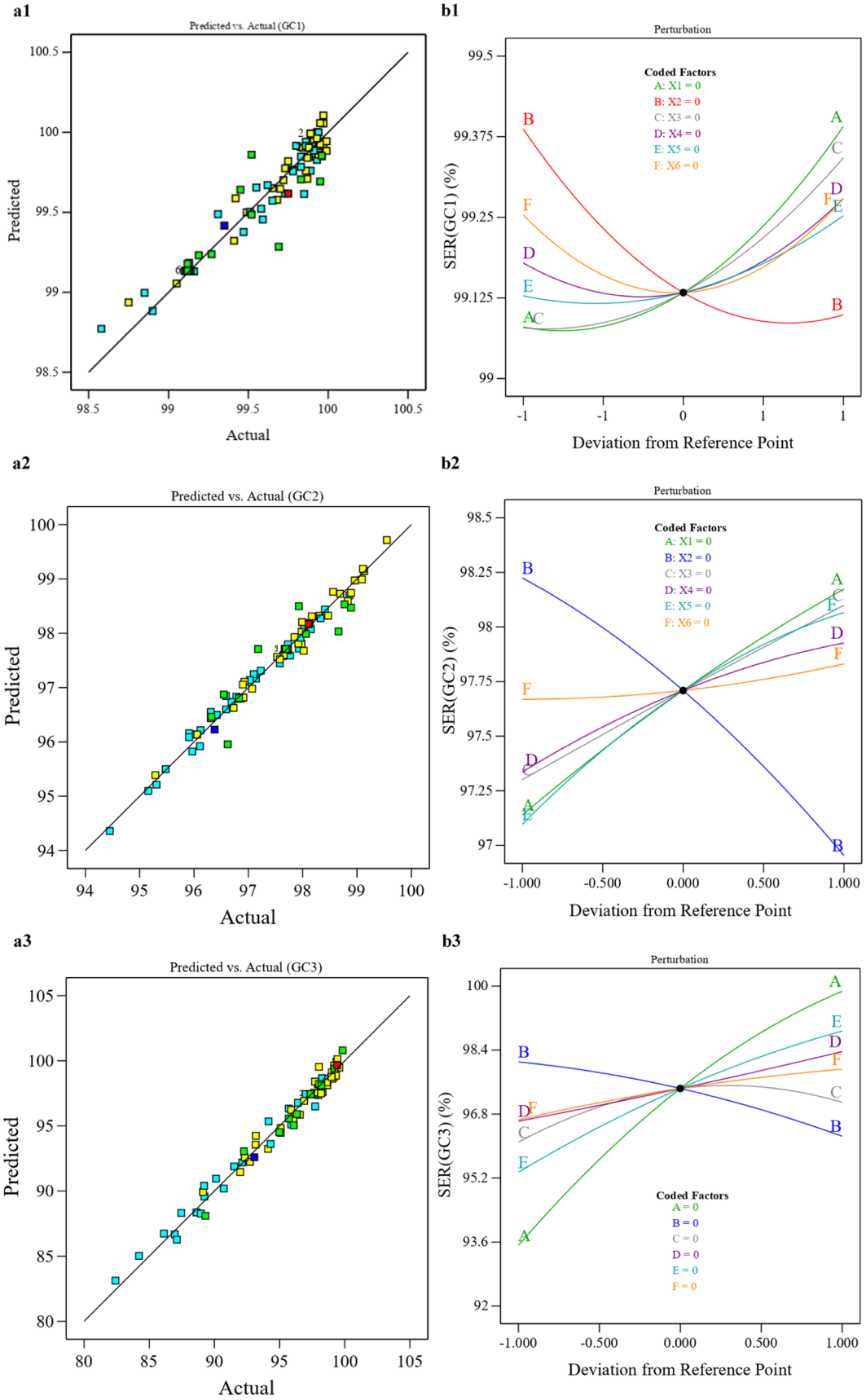

Figure 3. Comparison of quadratic model results and corresponding experimental data: (a) model-predicted vs actual efficiency and (b) diversion plot of the model.

https://doi.org/10.1021/acsomega.3c05193
ACS Omega 2023, 8, 42522−42539

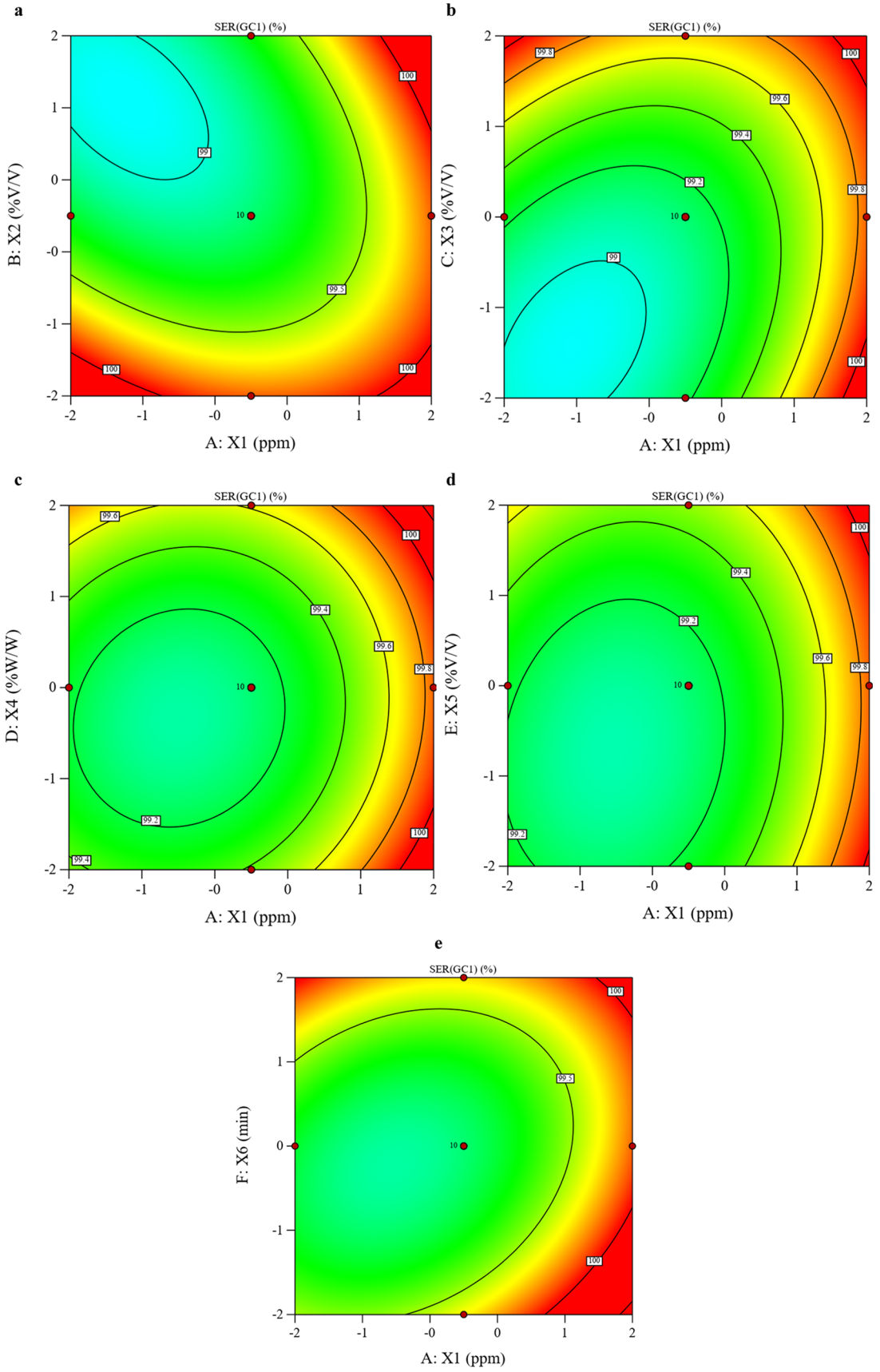

Figure 4. Mutual effects of sulfur (mercaptan) content of *n*-heptane (i.e., gas condensate) against hydrogen peroxide (a), formic acid (b), phosphotungstic acid (c), isobutyl alcohol (d), and ultrasonication time (e) in terms of desulfurization efficiency.

https://doi.org/10.1021/acsomega.3c05193
ACS Omega 2023, 8, 42522−42539

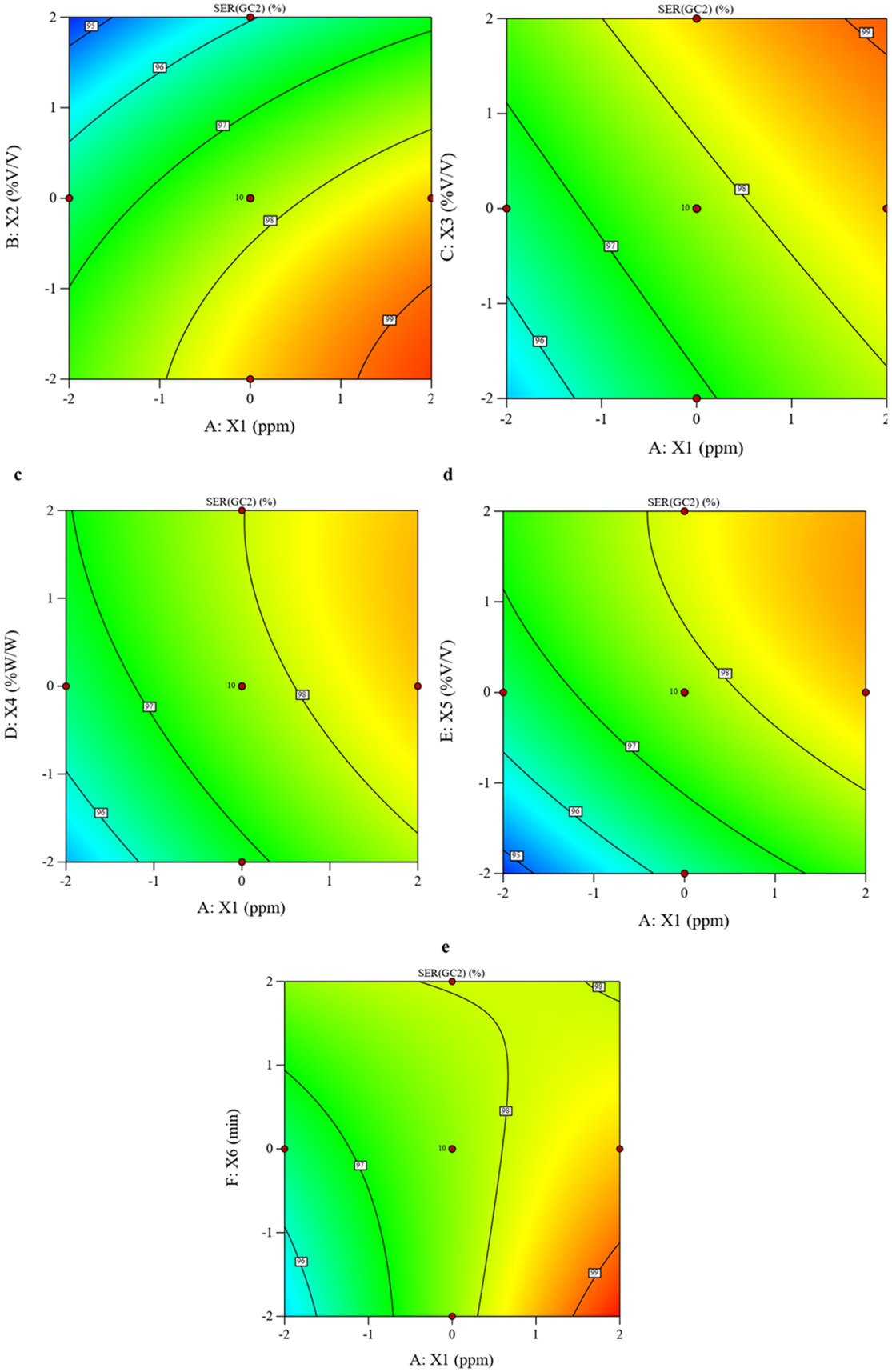

Figure 5. Mutual effects of sulfur (sulfide) content of *n*-heptane (i.e., gas condensate) against hydrogen peroxide (a), formic acid (b), phosphotungstic acid (c), isobutanol (d), and ultrasonication time (e) in terms of desulfurization efficiency.

https://doi.org/10.1021/acsomega.3c05193
ACS Omega 2023, 8, 42522−42539

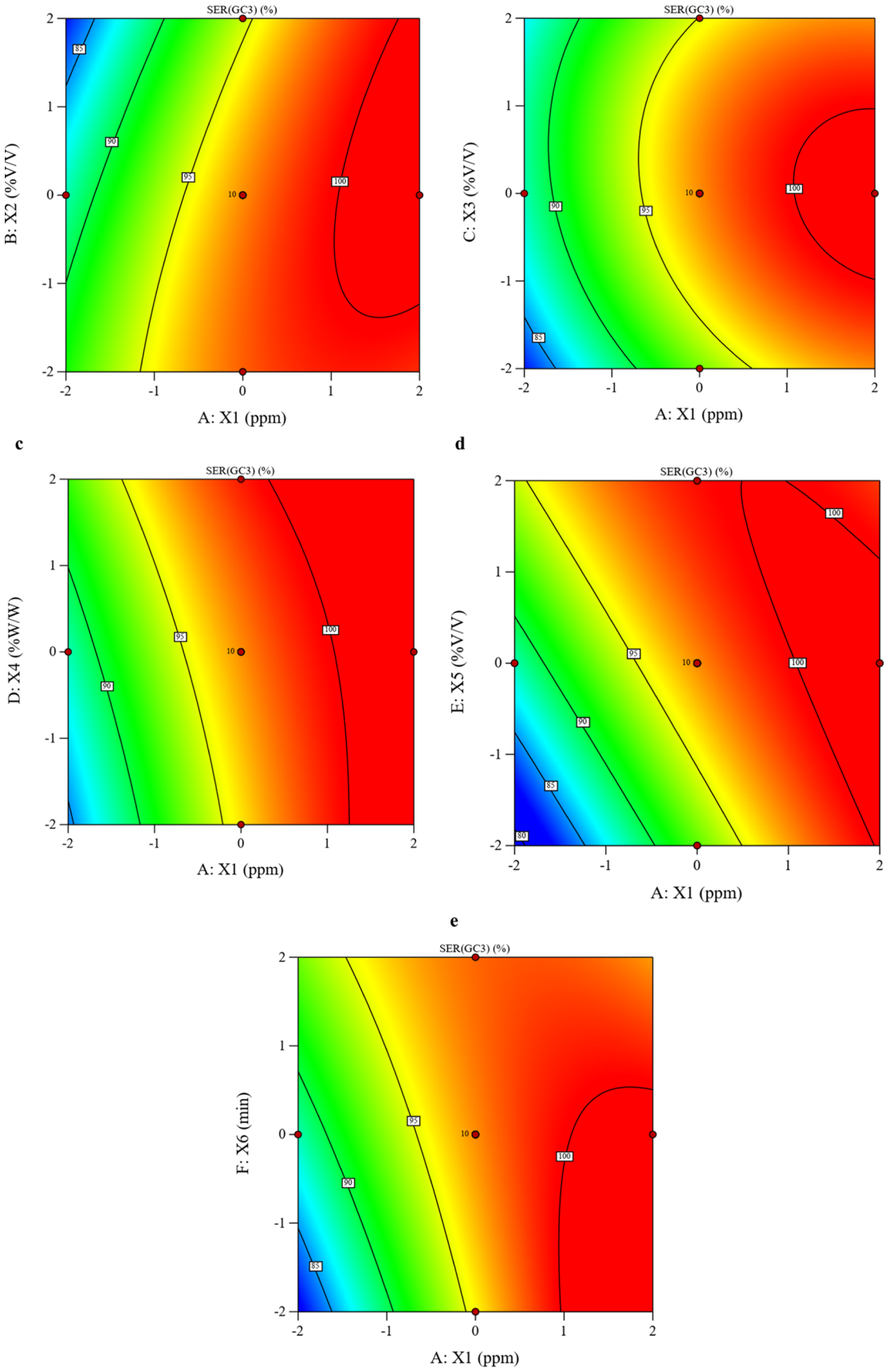

Figure 6. Mutual effects of sulfur (thiophene) content of *n*-heptane (i.e., gas condensate) against hydrogen peroxide (a), formic acid (b), phosphotungstic acid (c), isobutanol (d), and ultrasonication time (e) in terms of desulfurization efficiency.

https://doi.org/10.1021/acsomega.3c05193
ACS Omega 2023, 8, 42522−42539

Table 7. Characteristics of the Industrial Gas Condensate

property	method	unit	IS_1	IS_2
Sp. Gr. 60/60 °F	ASTM D4052		0.740	0.732
total sulfur	ASTM D7039	ppm (wt %)	1726.30	1521.87
mercaptans	ASTM D3227	ppm (wt %)	2400	2243
H_2S	ASTM D1159	ppm (wt %)	20	5

polyoxometalate acid then forms a proxy-metal complex with active oxygen, which binds with isobutyl alcohol, a phase transfer agent, and is transferred to the organic phase. The sulfurous compounds are then oxidized by the proxy metals, resulting in the production of sulfones in the aqueous phase. The reduced proxy-metal compound in the ionic phase undergoes ion exchange with the phase transfer agent and is then returned to the aqueous phase where it is reoxidized by hydrogen peroxide. This cycle continues until all sulfur or oxidizer is consumed. Emulsion induction by UAOD facilitates the phase transfer of the metal-proxy complex and isobutanol.

3.5. Analysis of the Contours. *3.5.1. Effect of Initial Mercaptan Content.* In Figure 4, the desulfurization efficiency of mercaptan (GC_1) is displayed as a function of the ratio of X_1 to X_6. As depicted in all of the figures, desulfurization efficiency improves with increasing mercaptan content. This is due to the fact that higher mercaptan content allows for greater selectivity of aqueous phase components to react with mercaptans, while also preventing side reactions of free radicals. At low sulfur content, free radicals are produced during the reaction of hydrogen peroxide and acid, which then react with each other to produce oxygen and water, thereby diluting the acid in the aqueous phase. In Figure 4(a), there are two distinguishable regions for the effect of hydrogen peroxide on desulfurization. Low sulfur content requires a low amount of hydrogen peroxide, while for high sulfur content, even low or high hydrogen peroxide levels have the same results, but the middle amounts decrease efficiency. Therefore, low dosages of hydrogen peroxide should be used in any case.

Hydrogen peroxide imposes dual negative and positive effects on desulfurization efficiency as it contributes in two mechanisms at the same time to form free radicals: (1) reaction with formic acid to produce performic acid and (2) reaction with phosphotungstic acid to form epoxy metals. Thus, the hydrogen peroxide content must be adjusted based on the formic acid and phosphotungstic acid contents. If the dosage of hydrogen peroxide exceeds the consumption rates of acids, the high reactivity of hydrogen peroxide leads to the release of oxygen and extra water, diluting the aqueous phase and suppressing the desulfurization efficiency.

In Figure 4(b), for low mercaptan levels, a higher promoter content leads to a higher desulfurization efficiency, while, at high sulfur levels, there is little effect. Similarly, in Figure 4(c), the catalyst (phosphotungstic acid) has a direct effect on desulfurization but with a much weaker intensity than in Figure 4(b). Phosphotungstic and formic acids compete with each other and follow two different mechanisms of desulfurization when reacting with hydrogen peroxide. The effect of the catalyst is smaller than that of formic acid, but this does not rule out the advantage of using the catalyst since it forms poly(polyoxometalate) to become a proxy-metal complex with active oxygen that can be transferred between the aqueous and organic phases. This indicates that the amount of phosphotungstic acid as a catalyst is directly and positively linked to the mercaptan content. It can be observed from Figure 4(c) that the catalyst has the greatest impact on the desulfurization efficiency only at low doses, and additional doses of the catalyst do not have a significant effect on the desulfurization efficiency. Therefore, it is recommended to use lower doses of the catalyst for mercaptan removal. Figure 4(d) indicates that a higher dosage of the phase transfer agent improves desulfurization. The phase transfer agent has one aqueous end and one organic end, which helps to connect the aqueous and organic phases, maintaining their continuous attachment. Ultrasonic waves play a significant role in connecting the two phases when ultrasonication is employed. The low slope of changes in the response with changing the phase transfer agent implies that the ultrasonic waves have a more significant impact on the response, which justifies the lower use of the phase transfer agent. Based on Figure 4(e), the best response is expected with the shortest ultrasonication time, with the desulfurization efficiency only slightly improving as the ultrasonication time increases. This demonstrates the advantage of ultrasonication, as it yields positive effects in a short amount of time.

3.5.2. Effect of Initial Sulfide Content. Figure 5(a) shows that increasing the sulfide content in *n*-heptane (GC_2) improves the efficiency of desulfurization. When there is an excess of sulfide in the hydrocarbon phase, the selectivity of the aqueous phase and the reactivity of sulfides increase, promoting the conversion of sulfidic compounds into sulfones and enhancing the desulfurization efficiency. However, when the sulfide content is low, the chances of secondary reactions increase, reducing the desulfurization efficiency. Figure 5(a)

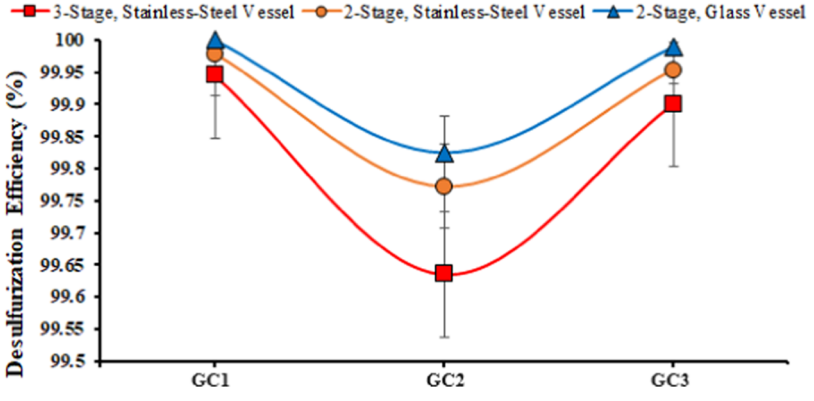

Figure 7. Effects of the number of extraction stages and vessel material on the desulfurization efficiency for synthetic gas-condensate samples containing mercaptans (GC_1), sulfides (GC_2), and thiophenes (GC_3).

https://doi.org/10.1021/acsomega.3c05193
ACS Omega 2023, 8, 42522−42539

Table 8. Experimental Results of the Synthetic and Industrial Samples Using the Optimal Conditions Obtained from the Proposed Model

	actual of variable						
system	X_1 (ppm)	X_2 (mol %)	X_3 (mol %)	X_4 (wt %)	X_5 (mol %)	X_6 (min)	results of experimental (2-stage, NNDMF solvent, glass vessel) (%)
GC_1	1357.6	48.0	69.7	8.9	5.6	11.3	99.93
IS_1	1726.3	23.9	38.2	21.2	4.4	36.3	97.96
IS_2	1521.8	10.0	40.5	9.0	4.3	31.5	99.13

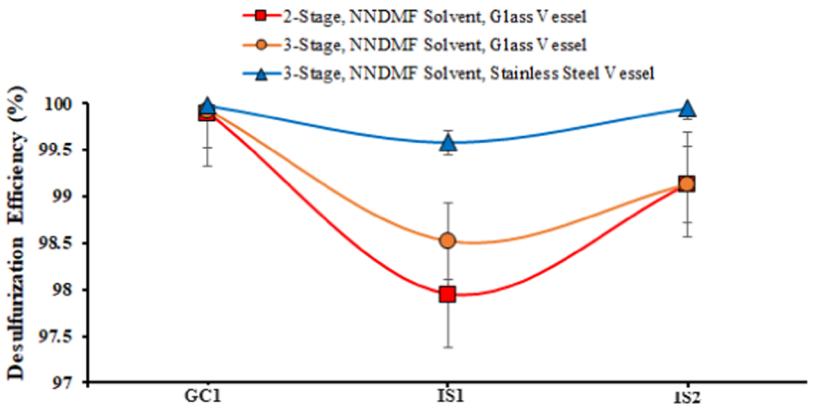

Figure 8. Comparison of the results of desulfurization between GC_1, IS_1, and IS_2 under optimal conditions for different numbers of extraction stages and reactor vessel materials.

also demonstrates that as the sulfur content increases, the amount of hydrogen peroxide needed decreases, depending on the dosages of the enhancer and the catalyst. The highest desulfurization efficiency occurs when there are high levels of sulfur (sulfide) and formic acid, as shown in Figure 5(b). Figure 5(c) indicates that the dosage of phosphotungstic acid, as the catalyst, is directly related to the sulfide content of the sample, following a trend similar to that for formic acid but at a slower rate. Furthermore, Figure 5(d) demonstrates that using a higher dosage of the phase transfer agent can enhance the desulfurization efficiency. Ultrasonication time is also a factor, as a long time allows for the accumulation of microemulsions in the oxidation reaction medium, increasing the contact surface between the aqueous and organic phases and thus promoting the conversion of sulfide compounds into sulfones. However, according to Figure 5(e), the optimal response is obtained with a minimal ultrasonication time.

3.5.3. Effect of Initial Thiophene Content. As the benzothiophene content in (GC_3) increased, Figure 6 demonstrated an improvement in the desulfurization efficiency. The experimental results indicated that higher sulfur contents in the gas-condensate sample resulted in a greater desulfurization efficiency, which may be due to the influence of ultrasonic waves. The removal efficiency of sulfur increased with the oxidant up to a certain level, regardless of the sulfur content of the sample, indicating a direct correlation between sulfur content and desulfurization efficiency. In Figure 6(a), it was observed that the desulfurization efficiency decreased as the hydrogen peroxide dosage increased for a given sulfur (thiophene compound) content, with the best results obtained at higher sulfur contents and lower hydrogen peroxide dosages. This could be attributed to an increase in the aqueous phase and the dependency of hydrogen peroxide dosage on enhancer and catalyst dosages. Therefore, optimal adjustment of hydrogen peroxide dosage was necessary. Figure 6(b) shows that at a given sulfur (thiophene) content, the desulfurization efficiency increased with formic acid dosage up to a certain level, beyond which it decreased due to the undesired effect of the aqueous phase and dependence of formic acid dosage on hydrogen peroxide dosage. This implied that the dosage of the two substances needed to be optimized to maintain the alkalinity of the sample within a certain range, with the best results obtained at higher sulfur contents and moderate formic acid dosages. Figure 6(c) demonstrates that desulfurization efficiency increased with increasing catalyst dosage (phosphotungstic acid), and a direct correlation was observed between the sulfur content and catalyst dosage. This was because a higher amount of polyoxometalate (a product of the reaction between hydrogen peroxide and phosphotungstic acid) provided for improved conversion of thiophene compounds to sulfones, thereby enhancing removal efficiency. In Figure 6(d), the most favorable results were obtained at higher concentrations of sulfur and the phase transfer agent. To enhance sulfur removal, isobutanol was utilized as a phase transfer agent to aid in the transfer of oxidized sulfur contents from the organic phase to the aqueous phase. Hence, the desulfurization efficiency rose with an increase in the isobutanol dosage. Figure 6(e) shows the impact of reaction time on the sulfur content. At lower sulfur contents, the desulfurization efficiency improved with an increase in ultrasonication time. However, at higher sulfur contents, the desulfurization efficiency increased only marginally with an extension in sonication time, indicating the need to optimize the sonication time. A lower demand for ultrasonication is implied as the higher the sulfur content of the sample, the faster the oxidation reaction occurs. These results indicate that all variables, such as the dosages of oxidant, enhancer, catalyst, and phase transfer agent, as well as the ultrasonication time, significantly depend on the content of thiophene compounds in the sample.

3.6. Optimization. The objective of the current research is to identify the most effective parameters for various sulfur contents. Optimization of the ultrasound-assisted oxidation technique involves reducing the oxidant consumption and

https://doi.org/10.1021/acsomega.3c05193
ACS Omega 2023, 8, 42522−42539

oxidation time while maintaining an efficiency level exceeding 99.99%. This necessitates optimization of the mathematical model with the aid of software. Design Expert software has the advantage of enabling users to determine optimal conditions for desulfurizing gas-condensate samples with sulfur content ranging from 100 to 3000 ppm. This allows for the estimation of desulfurization efficiency under specific conditions, unlike previous studies that only focused on the sulfur content of particular wells. The present research provides optimal conditions for different levels of sulfur content, enabling estimation of the anticipated desulfurization efficiency under optimal conditions. Through mathematical modeling, the software determined 100 optimal points that had the same level of desirability, with example optimal points shown in Table 7. By conducting experiments under the optimal conditions of Table 7, the maximum efficiency of sulfur removal for mercaptan, sulfide, and thiophene compounds was 99.93, 99.63, and 99.81%, respectively.

3.7. Effect of the Extraction Stage and Reactor Vessel Material. Figure 7 shows that the maximum efficiency was achieved when the reactor vessel material was changed from glass to stainless steel. Therefore, the findings revealed the significance of the ultrasonic container material, with metal containers exhibiting greater wave transmission to the sample, resulting in an increase in removal efficiency (red color curve). Additionally, it was observed that as the number of extraction steps increased, the removal efficiency also increased (green color curve than the blue color one). However, the increase in yield during the third stage was not significantly notable compared to the second stage. Thus, it is advisable to augment the number of extraction steps only in situations where the complete elimination of sulfur is necessary.

3.8. Field Data. Using Design Expert software, the optimal operating conditions were extracted for desulfurization of both industrial samples, as demonstrated in Table 8. Based on the results (Figure 8), it was found that using two-stage extraction with DMF (with a solvent-to-hydrocarbon ratio of 2:1) on IS_1 and IS_2 resulted in desulfurization efficiencies of 97.96 and 99.13%, respectively. To enhance the mercaptan removal efficiency under optimal conditions, the number of extraction stages was increased from two to three and also the reactor vessel material was switched from glass to stainless steel. These modifications led to desulfurization efficiencies of 99.61 and 99.98% for IS_1 and IS_2, respectively, as depicted in Figure 8. These outcomes underscored the effectiveness of UAOD for mercaptan removal. The results verified that the model accurately identified the optimal conditions for desulfurization and accurately predicted its efficiency. The negligible disparity in mercaptan removal efficiency between the synthetic gas condensate (GC_1, 100%) and industrial sample was due to the presence of hydrogen sulfide in the industrial gas-condensate sample.

4. CONCLUSIONS

In this research, UAOD was utilized for removing sulfurous compounds from gas condensates. Results show that the best combination of the mixture in removing different sulfurous compounds is hydrogen peroxide as the optimal oxidant, formic acid as the optimal promoter, phosphorus tungstic acid as the optimal catalyst, and isobutanol as the optimal phase transfer agent. Experimental results showed that most of the sulfur content was removed upon the first extraction stage, with the two-stage and three-stage extraction procedures returning more or less the same results (at each stage, the solvent-to-gas-condensate ratio was set to 1:2). At optimal points, the GC_1, GC_2, and GC_3 models (under two-stage extraction in a glass-made sonoreactor vessel) ended up removing the sulfurous compounds at 99.93, 99.63, and 99.86%, respectively. To enhance the removal efficiency, three extraction stages were practiced in a stainless-steel reactor vessel, which led to 100% removal of mercaptans, 99.81% removal of sulfides, and 99.94% removal of benzothiophene. The desulfurization efficiency of 99.98% on industrial gas-condensate sample 2 confirmed the validity of the mathematical modeling. The results provide for determining optimal conditions for different levels of sulfur content in the gas condensate and conversely predict the achievable desulfurization efficiency under a given set of conditions.

AUTHOR INFORMATION

Corresponding Author

Maryam Asemani − *Department of Chemical Engineering College of Engineering 2, Shiraz Branch, Islamic Azad University, Shiraz 7198774731, Iran*; Email: masemani@gmail.com

Authors

Ameneh Taghizadeh − *Department of Chemical Engineering College of Engineering 2, Shiraz Branch, Islamic Azad University, Shiraz 7198774731, Iran*

Feridun Esmaeilzadeh − *Department of Chemical Engineering, School of Chemical, Petroleum and Gas Engineering, Shiraz University, Shiraz 7193616511, Iran*

Abolhasan Ameri − *Department of Chemical Engineering College of Engineering 2, Shiraz Branch, Islamic Azad University, Shiraz 7198774731, Iran*

Complete contact information is available at: https://pubs.acs.org/10.1021/acsomega.3c05193

Notes

The authors declare no competing financial interest.

ACKNOWLEDGMENTS

The authors are grateful to Shiraz Branch, Islamic Azad University, and Shiraz University for supporting this research.

REFERENCES

(1) Liu, S.; Liu, Z.; Zhu, H.; et al. The Roles of Red Mud as Desulfurization and Denitrification in Flue Gas: A review. *J. Environ. Chem. Eng.* **2023**, *11*, No. 109770.

(2) Topsøe, H.; Clausen, B. S.; Massoth, F. E. *Hydrotreating Catalysis*; Springer, 1996.

(3) Ma, X.; Sakanishi, K.; Mochida, I. Hydrodesulfurization reactivities of various sulfur compounds in vacuum gas oil. *Ind. Eng. Chem. Res.* **1996**, *35* (8), 2487−2494.

(4) Vradman, L.; Landau, M.; Herskowitz, M. Deep desulfurization of diesel fuels: kinetic modeling of model compounds in trickle-bed. *Catal. Today* **1999**, *48* (1−4), 41−48.

(5) Soleimani, M.; Bassi, A.; Margaritis, A. Biodesulfurization of refractory organic sulfur compounds in fossil fuels. *Biotechnol. Adv.* **2007**, *25* (6), 570−596.

(6) Chen, T.-C.; Shen, Y. H.; Lee, W. J.; et al. An economic analysis of the continuous ultrasound-assisted oxidative desulfurization process applied to oil recovered from waste tires. *J. Cleaner Prod.* **2013**, *39*, 129−136.

https://doi.org/10.1021/acsomega.3c05193
ACS Omega 2023, 8, 42522−42539

(7) Wan, M.-W.; Yen, T.-F. Enhance efficiency of tetraoctylammonium fluoride applied to ultrasound-assisted oxidative desulfurization (UAOD) process. *Appl. Catal., A* **2007**, *319*, 237−245.
(8) Ali, M. F.; Almalki, A.; Elali, B.; et al. Deep desulphurization of gasoline and diesel fuels using non-hydrogen consuming techniques. *Fuel* **2006**, *85* (10−11), 1354−1363.
(9) Salem, H. M.; Abdelrahman, A. A. Sono-catalytic oxidative desulfurization of fuels using Fe6W18O70@ ZrFe2O5. *J. Alloys Compd.* **2023**, *956*, No. 170275.
(10) Pouladi, B.; Fanaei, M. A.; Baghmisheh, G. Optimization of oxidative desulfurization of gas condensate via response surface methodology approach. *J. Cleaner Prod.* **2019**, *209*, 965−977.
(11) Alibolandi, M.; Darian, J. T.; Ghaedian, M.; et al. Non-catalytic oxidative desulfurization of gas condensate by ozone and process optimization using response surface methodology. *Korean J. Chem. Eng.* **2020**, *37*, 1867−1877.
(12) Sinhmar, P. S.; Gogate, P. R. Ultrasound assisted oxidative desulfurization of simulated diesel using flow cell and longitudinal bath in combination with different oxidants. *Chem. Eng. Process.* **2020**, *153*, No. 107968.
(13) Mofidi, M.; Shahhosseini, S. Ultrasound assisted oxidative desulfurization of a model fuel using a deep eutectic solvent: Optimization and experimental design. *Chem. Eng. Process.* **2022**, *171*, No. 108724.
(14) Desai, K.; Dharaskar, S.; Khalid, M.; et al. Triphenyl methyl phosphonium tosylate as an efficient phase transfer catalyst for ultrasound-assisted oxidative desulfurization of liquid fuel. *Environ. Sci. Pollut. Res.* **2021**, *28*, 26747−26761.
(15) Fan, J.; Chen, A.; Saxena, S.; et al. Ultrasound-assisted oxidative desulfurization of Arabian extra light oil (AXL) with molecular characterization of the sulfur compounds. *Fuel* **2021**, *305*, No. 121612.
(16) Yu, W.; Luo, Z.; Javadpour, F.; et al. Sensitivity analysis of hydraulic fracture geometry in shale gas reservoirs. *J. Pet. Sci. Eng.* **2014**, *113*, 1−7.
(17) Shayegan, Z.; Razzaghi, M.; Niaei, A.; et al. Sulfur removal of gas oil using ultrasound-assisted catalytic oxidative process and study of its optimum conditions. *Korean J. Chem. Eng.* **2013**, *30*, 1751−1759.
(18) Zhang, J.; Sun, S.; Bian, Y.; et al. Adsorptive desulfurization of metal phthalocyanine functionalized poly-ionic liquids grafted to silica gel. *Fuel* **2018**, *220*, 513−520.
(19) Zheng, D.; Zhu, W.; Xun, S.; et al. Deep oxidative desulfurization of dibenzothiophene using low-temperature-mediated titanium dioxide catalyst in ionic liquids. *Fuel* **2015**, *159*, 446−453.
(20) Jiao, J.; Zhou, X.; Zhao, S.; et al. In situ highly dispersed loading of molybdenum dioxide with oxygen vacancies on N-doped graphene for enhanced oxidative desulfurization of fuel oil. *J. Environ. Chem. Eng.* **2023**, *11* (2), No. 109402.
(21) Lü, H.; Li, P.; et al. Deep catalytic oxidative desulfurization (ODS) of dibenzothiophene (DBT) with oxalate-based deep eutectic solvents (DESs). *Chem. Commun.* **2015**, *51* (53), 10703−10706.
(22) Liu, B.; Liu, L.; Wang, Z.; et al. Effect of hydrogen spillover in selective hydrodesulfurization of FCC gasoline over the CoMo catalyst. *Catal. Today* **2017**, *282*, 214−221.
(23) Mei, H.; Mei, B.; Yen, T. F. A new method for obtaining ultra-low sulfur diesel fuel via ultrasound assisted oxidative desulfurization. *Fuel* **2003**, *82* (4), 405−414.
(24) Ibrahim, N. K.; Noori, W. A.; Khasbag, J. M. Ultrasound-Assisted Oxidative Desulfurization of Diesel. *J. Eng.* **2023**, *22* (11), 55−67.
(25) Zhao, M.; Han, P.; Lu, X. Ultrasound assisted photocatalytic oxidative desulfurization of model diesel fuel. *Pet. Sci. Technol.* **2018**, *36* (1), 29−33.
(26) Babushkina, E. A.; Belokopytova, L. V.; Grachev, A. M.; et al. Variation of the hydrological regime of Bele-Shira closed basin in Southern Siberia and its reflection in the radial growth of Larix sibirica. *Reg. Environ. Change* **2017**, *17*, 1725−1737.
(27) Gildo, P. J.; Dugos, N.; Roces, S.; Wan, M.-W. Optimized Ultrasound-Assisted Oxidative desulfurization process of simulated fuels over activated carbon-supported phosphotungstic acid. *MATEC Web Conf.* **2018**, *156*, No. 03045, DOI: 10.1051/matecconf/201815603045.
(28) Margeta, D.; Sertić-Bionda, K.; Foglar, L. Ultrasound assisted oxidative desulfurization of model diesel fuel. *Appl. Acoust.* **2016**, *103*, 202−206.
(29) Dai, Y.; Qi, Y.; Zhao, D.; Zhang, H. An oxidative desulfurization method using ultrasound/Fenton's reagent for obtaining low and/or ultra-low sulfur diesel fuel. *Fuel Process. Technol.* **2008**, *89* (10), 927−932.
(30) Duarte, F. A.; de A Mello, P.; Bizzi, C. A.; et al. Sulfur removal from hydrotreated petroleum fractions using ultrasound-assisted oxidative desulfurization process. *Fuel* **2011**, *90* (6), 2158−2164.
(31) Shamseddini, A.; Esmaeilzadeh, F.; Mowla, D. Diesel Oil Upgradation by Ultrasound Irradiation: A Study on the Effects of Main Operational Parameters. *Phys. Chem. Res.* **2017**, *5* (4), 691−707.
(32) Wan, M.-W.; Biel, L. C. C.; Lu, M. C.; et al. Ultrasound-assisted oxidative desulfurization (UAOD) using phosphotungstic acid: effect of process parameters on sulfur removal. *Desalin. Water Treat.* **2012**, *47* (1−3), 96−104.

https://doi.org/10.1021/acsomega.3c05193
ACS Omega 2023, 8, 42522−42539